

Operational Aspects of the MI Large Aperture Quadrupole (WQB)

W. Chou, September 2006

Abstract

A two-year Large Aperture Quadrupole (WQB) Project was completed in the summer of 2006. Nine WQBs were designed, fabricated and bench-tested by the Technical Division [1]. Seven of them were installed in the Main Injector and the other two for spares. They perform well. The aperture increase meets the design goal and the perturbation to the lattice is minimal. The machine acceptance in the injection and extraction regions is increased from 40π to 60π mm-mrad. This note is a report from users' point of view.

Outline

1. Introduction
 2. WQB parameters
 3. Field quality requirement
 4. Field correction and trim current table
 5. BPM offset tables
 6. Orbit measurement
 7. Machine aperture and acceptance improvement
 8. Acknowledgement
 9. References
- Appendix: Locations and end views of the installed WQBs

1. Introduction

It is known that the injection and extraction areas with Lambertson magnets are the bottleneck of the Main Injector. The physical aperture in these areas is cut to half as shown in Figure 1. The transverse acceptance is limited to 40π mm-mrad. Significant beam losses have been observed in these areas during high intensity operation.

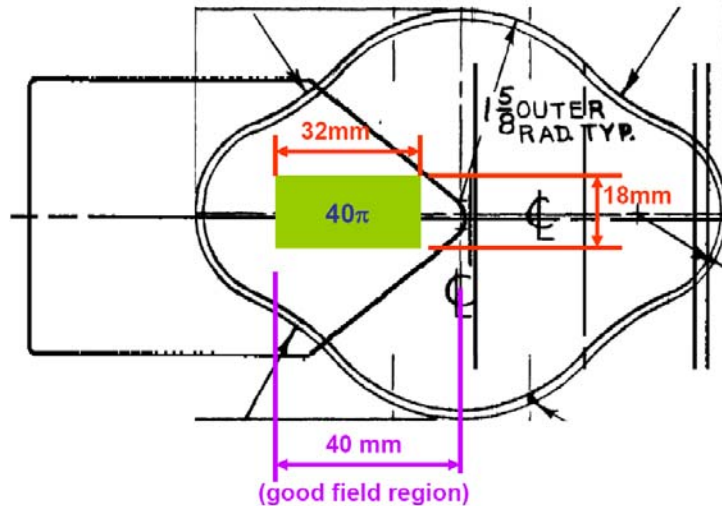


Figure 1: Physical aperture and machine acceptance in the Lambertson area.

In order to enlarge the aperture and reduce beam loss, it was decided to replace the quadrupoles in these areas by new ones (called WQB) that will have a larger aperture. The project started in early 2004 in collaboration between the Accelerator Division and Technical Division. The scope of this project was defined as follows:

- To design, fabricate and bench-test nine WQBs
- To design, fabricate and calibrate nine extra-wide aperture (EXWA) BPMs
- To install seven WQBs and seven new BPMs in the MI during 2006 shutdown (the rest for spares)
- To install seven trim coil power supplies
- To commission the WQBs and new BPMs

The project was completed in the summer of 2006. Table 1 lists the location of the WQBs, new BPMs and old quads. Most of the removed old quads are radioactively hot due to heavy beam losses in these areas. All seven installed WQBs perform well and meet the design goals. The aperture is increased by 10 mm as expected. The machine acceptance in the injection and extraction regions is increased from 40π to 60π mm-mrad. Thanks to careful correction of the field strength by trim coils during the cycle, the perturbation to the lattice is minimal.

Table 1: WQB, EXWA BPM and the Old Quad

Location	WQB Serial No.	EXWA BPM Serial No.	Old Quad Serial No.	Old Quad Radioactivity
Q101	WQB 001	EXWA 01	IQG 333	CLASS 2
Q222	WQB 007	EXWA 07	IQB 045	CLASS 2
Q321	WQB 006	EXWA 08	IQB 071	CLASS 1
Q402	WQB 004	EXWA 04	IQE 065	CLASS 3
Q522	WQB 003	EXWA 02	IQE 072 (*)	CLASS 2 (*)
Q608	WQB 005	EXWA 05	IQE 225	CLASS 2
Q620	WQB 002	EXWA 06	IQE 134	CLASS 3

(*) IQE 072 was relocated from Q522 to Q521. The old quad at Q521 was IQB 177, which was removed from the ring and is a CLASS 2 magnet.

Figure 2 shows a WQB installed in the Main Injector. There is a transition piece connecting the star-shaped beam pipe inside the WQB and the regular elliptical pipe. It serves the purpose for reducing the beam coupling impedance and was installed wherever space permitted. These transition pieces were heat treated prior to the installation in order to keep the permeability of the welding below 1.01. (It was greater than 1.1 before heat treatment.)



Figure 2: A large aperture quad (WQB) installed at the Q222 location.

2. WQB Parameters

It is desirable to make the aperture of the new quads as large as possible. However, there are several constraints:

- The WQB must have the same integrated field strength $B'L$ as the regular quadrupole (IQB):

$$\left(\mu_0 \frac{NI}{r^2} L \right)_{\text{WQB}} = \left(\mu_0 \frac{NI}{r^2} L \right)_{\text{IQB}}$$

Because WQBs and IQBs are on the same bus (i.e. same I) and have the same effective length L , the radius r must satisfy:

$$\frac{r_{\text{WQB}}}{r_{\text{IQB}}} = \left(\frac{N_{\text{WQB}}}{N_{\text{IQB}}} \right)^{1/2}$$

In other words, the increase of the aperture is a function of the turn number N and is step-wise rather than continuous.

- The pole tip field increases linearly with the aperture. In order to keep field saturation under control, for given field gradient the maximum allowable aperture is limited.

The Technical Division investigated several types of steel and selected one with the best saturation behavior. Based on its $B-H$ curve, it was decided to increase the turn number from 4 (for IQB) to 7 (for WQB). The corresponding aperture increase is $(7/4)^{1/2} = 1.32$, i.e. from $2r = 3.286''$ (IQB) to $4.347''$ (WQB). The main parameters are listed in Table 2.

Table 2: WQB Parameters

Aperture	4.347''
Length	84''
Max gradient at 150 GeV/c	19.6 T/m
Good field region	±2''
Turns per pole	7
Peak current at 150 GeV/c	3540 A
RMS current	2000 A
Resistance	8.1 mΩ
Inductance	3.7 mH
Trim coil turns per pole	18
Max trim current	28 A
Weight	12,000 lb

3. Field Quality Requirement

It is essential for the WQB to maintain the same integrated strength as the IQB during the ramp. The beta-wave and tune shift from field errors can be estimated by using the first order perturbation method. Assume a thin quadrupole at location 1 with strength:

$$q = \frac{\int Gdl}{B\rho}$$

Then the beta-wave at location 2 and tune shift are, respectively:

$$\frac{\Delta\beta_2}{\beta_2} = q \times \beta_1 \times \sin 2\Psi$$

$$\Delta\nu = \frac{1}{4\pi} \times q \times \beta_1$$

where Ψ is the phase advance between 1 and 2. For the MI, one WQB with 1% integrated field error would give:

$$q = 0.001 \text{ m}^{-1}$$

$$\frac{\Delta\beta_2}{\beta_2} = 0.057$$

$$\Delta\nu = 0.0045$$

There are five horizontal focusing WQBs and two vertical focusing WQBs. In order to minimize the beta-wave and tune shift, the allowable field error was set to 0.1%, or 10 units (1 unit = 10^{-4}).

4. Field Correction and Trim Current Table

Because of its large aperture the WQB has much smaller higher order multipoles (HOM) than the IQB. However, the integrated field error was significant as shown in Figure 3. It reaches +4% at low current and -3% at high current. The errors at high current are from stronger saturation due to larger aperture, which was expected. The

errors at low current come from the fact that, because the steel was chosen for its better saturation behavior, we pay a price for its worse hysteresis property. Addition or removal of magnet end shims does not help because it would only move the whole curve up or down.

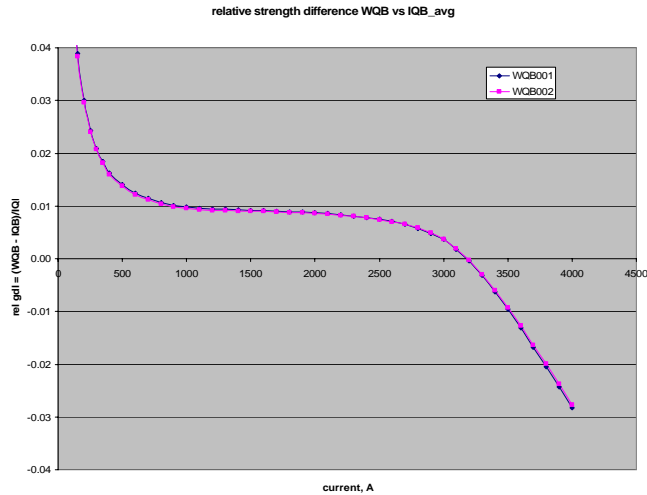


Figure 3: Relative strength difference between the WQB and average IQB.

These errors must be corrected by the trim coil. There are two important details that must be taken into account in calculating the required trim current.

1) Magnet reset current:

During the cycle, the quadrupole current does not go to zero. The reset current is 150 A. Because the hysteresis behavior has strong dependence on the reset current, the WQB was measured at different reset current and the field was compared with IQB310, the only IQB of which the hysteresis data was available. The results are shown in Figure 4. It is seen the difference between the dark blue (150 A reset) and pink curves (zero reset) can be as big as 1%, which has to be corrected.

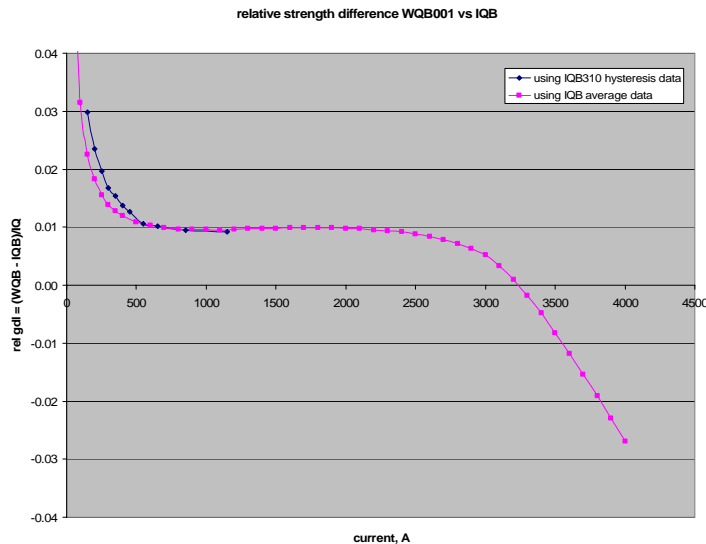


Figure 4: Relative strength difference between WQB and average IQB at zero reset (pink) and between WQB and IQB310 at 150 A reset (dark blue).

2) Trim coil transfer function anomaly:

The turn ratio of the trim coil to the main coil is 18/7. However, the measured transfer function ratio of the two coils shows some anomaly, especially at high current which reaches about +5% as listed in Table 3. This also needs to be taken into account.

Table 3: Trim Coil Transfer Function Anomaly (Courtesy M. Tartaglia)

Main Current (A)	Anomaly (negative trim polarity)	Anomaly (positive trim polarity)
200	1.20%	1.12%
1000	0.64%	0.54%
2800	0.94%	1.37%
3600	4.41%	4.97%

The calculated trim current, taking into account reset current and anomaly, is shown in Figure 5. The dark blue curve is for compensating the hysteresis errors at low current, the pink curve for the rest of the ramp. A smooth transition occurs at 650 A. The setting at about a score of operation points is listed in Table 4 and also shown in Figure 5. There are small differences between H quads (even number WQBs in Table 4 and yellow dots in Fig. 5) and V quads (odd number WQBs in Table 4 and light blue dots in Fig. 5). This is because the tunes are slightly different in the two planes ($v_H = 26.4$, $v_V = 25.4$). The accuracy of the trim power supply is 1%.

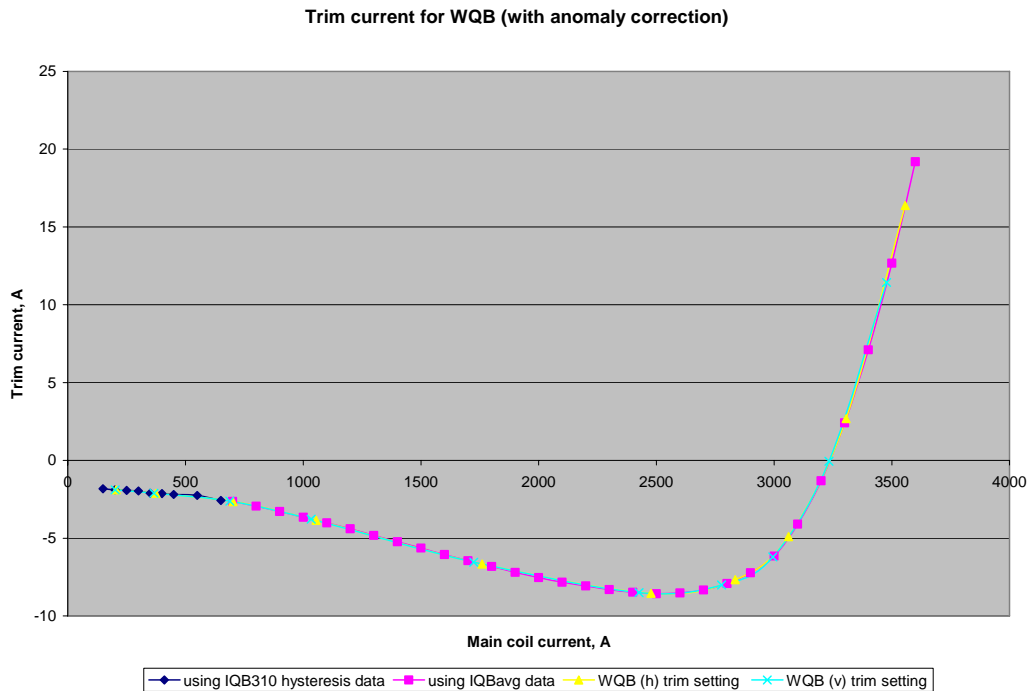


Figure 5: The required trim current during the ramp, including the hysteresis effect and transfer function anomaly. The operational setting points are shown in yellow (for H quads) and light blue (for V quads) with the values listed in Table 4.

Table 4: Trim Current Setting during the Ramp

Momentum (GeV/c)	Trim current (A)	
	WQB 222, 402, 522, 608, 620	WQB 101, 321
8.882	-1.894	-1.891
8.9494	-1.895	-1.892
9.0999	-1.898	-1.895
9.4993	-1.905	-1.901
9.9974	-1.914	-1.911
11.497	-1.941	-1.937
13.997	-2.037	-2.018
16	-2.116	-2.112
30	-2.643	-2.622
45	-3.854	-3.778
75	-6.668	-6.538
105	-8.547	-8.498
120	-7.667	-8.005
130	-4.902	-6.213
140	+2.689	-0.062
150	+16.385	+11.433

5. BPM Offset Tables

Nine extra wide aperture (EXWA) BPMs were designed and fabricated by the Mechanical Support Department and calibrated by the Instrumentation Department. Figure 6 is a picture. Unlike the existing BPM, each new BPM is able to measure both horizontal and vertical beam positions.

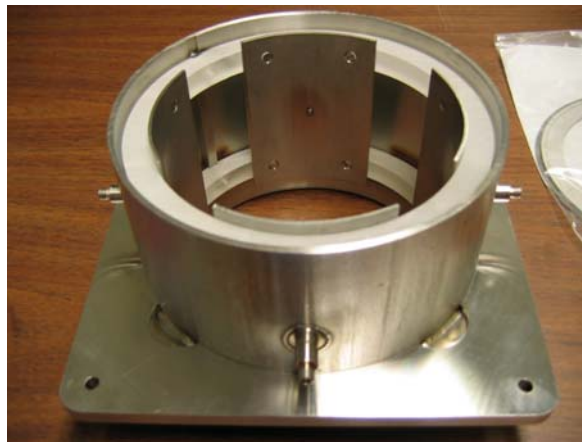


Figure 6: An extra wide aperture BPM with electrode ID = 5.625” and extended angle of each electrode = 60°.

In order for the BPM to measure the beam position accurately, its offset relative to the nearby quadrupole center must be corrected. (Note: The offset between the WQB lamination center and field center is less than 0.2 mm as measured by the stretched wire method.) This is done by means of an offset table in the database. There are four different types of offset.

- 1) Survey offset – the offset between the mechanical center of the BPM and that of the nearby quad. The data was provided by the Survey Group during installation and is listed in Table 5.

Table 5: Survey Offset

Location	Horizontal (mm)	Vertical (mm)	Roll (mrad)
BPM101 (WQB001)	-0.108	-0.751	-0.13
BPM222 (WQB007)	+0.143	-0.775	+0.54
BPM321 (WQB006)	+1.143	-1.301	-0.85
BPM402 (WQB004)	+0.552	-0.178	-0.25
BPM522 (WQB003)	+1.209	-1.826	+0.41
BPM608 (WQB005)	-0.339	+0.547	+0.47
BPM620 (WQB002)	+0.322	-1.556	+0.67
Q521	+0.178	+0.229	-1.04

Sign convention

Horizontal: + pointing inward (namely, facing the proton direction, the left-hand-side is positive);

Vertical: + pointing upward;

Roll: + indicating clockwise roll relative to proton direction.

- 2) BPM offset – the offset between the electrical and mechanical center of the BPM. The calibration was done by the Instrumentation Department and is listed in Table 6.

Table 6: BPM Offset

Location	Horizontal (mm)	Vertical (mm)
BPM101 (EXWA01)	-0.0703	+0.1373
BPM222 (EXWA07)	-0.0232	-0.1918
BPM321 (EXWA08)	+0.0535	-0.0846
BPM402 (EXWA04)	-0.2485	+0.2421
BPM522 (EXWA02)	+0.0217	+0.0809
BPM608 (EXWA05)	+0.1516	+0.2693
BPM620 (EXWA06)	-0.0723	-0.0138

Sign convention

Horizontal: + pointing outward (namely, facing the proton direction, the right-hand-side is positive);

Vertical: + pointing upward.

- 3) Electrical offset – the offset due to cables, jump boxes and electronics upstairs in the service building. There was a major task by the Instrumentation Department to measure this offset in the past year, not just for the EXWA BPMs but for all BPMs in the MI. For each BPM, the gain difference between A and B in a pair of long cables from the jump box to upstairs was measured and documented [2]. Additional difference from the electronics upstairs was calibrated to zero. The contributions from the jump box and the short cable connecting the BPM pickup to the box were considered to be small and ignored. Table 7 lists the cable gain difference of the new BPMs.

Table 7: Electrical Offset from Cable Gain Difference (Ref. [2])

Location	2.5MHz B/A xmsn	53MHz B/A xmsn
I:HP101	0.9993	0.9907
I:HP222	1.002	0.9868
I:HP321	0.9984	0.9871
I:HP402	0.9942	0.9986
I:HP522	1.002	0.9975
I:HP608	0.9961	0.9944
I:HP620	0.9981	1.014
I:VP101	0.9989	0.9907
I:VP222	0.9983	0.9868
I:VP321	0.9993	0.9871
I:VP402	0.999	0.9986
I:VP522	1	0.9975
I:VP602	0.9991	0.9944
I:VP620	1.002	1.014

Convention

Compensation by multiplying “A” beam signal amplitudes by the respective values in this listing.

- 4) Orbit offset – the intentional offset during the quadrupole installation in order to accommodate large beam orbit deflection in these areas. These numbers remain unchanged from the previous database.

The correction is performed in the following way:

$$H \text{ position} = \text{measured position} + \text{bpm offset} - \text{survey offset} + \text{orbit offset}$$

$$V \text{ position} = \text{measured position} + \text{bpm offset} + \text{survey offset}$$

where the measured position includes the compensation of the electrical offset 3).

6. Orbit Measurement

The simple geometry of the EXWA BPM makes it possible to use an analytical formula to compute the beam position from BPM signal [3]:

$$\text{pos (mm)} = A \times R \text{ (mm)} \times \frac{1 - \sqrt{1 - x^2}}{x}$$

where R is the BPM electrode radius (71.4375 mm), A is a constant to be fit to the calibration data, and x is the ratio of the signal difference to the signal sum. There is also another scaling formula suggested by Webber. He used MATHCAD to fit the bench calibration data and obtained a 5th order polynomial [4]:

$$\text{pos (mm)} = 43.513x + 5.432x^3 + 21.071x^5$$

Both formulae were used for data processing and compared with the calibration data. The results are shown in Figures 7 (horizontal) and 8 (vertical).

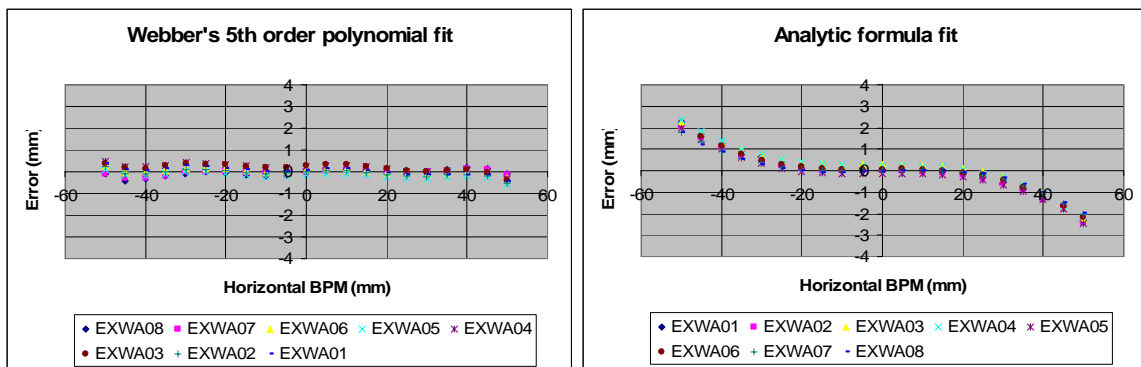


Figure 7: Differences between the horizontal bench measurement and fitting formulae. Left – the 5th order polynomial fit; right – the analytical formula fit.

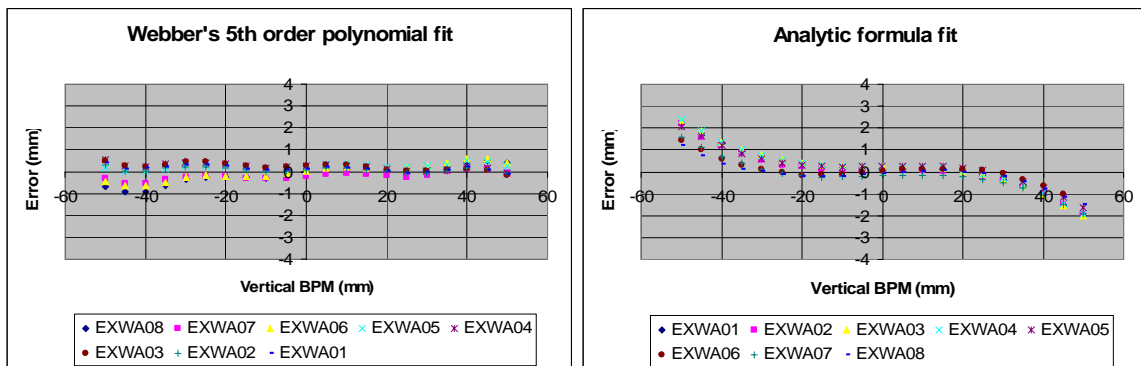


Figure 8: Differences between the vertical bench measurement and fitting formulae. Left – the 5th order polynomial fit; right – the analytical formula fit.

While the analytical formula is more accurate at small amplitude (< 20 mm), the 5th order polynomial fits much better at large amplitude (> 20 mm). Because the beam displacement is big at the WQB locations, it was decided to use the polynomial for data processing.

After installation, two measurements were carried out to verify the accuracy of these new BPMs, one using 3-bump method, another 1-bump method. Both methods are based on the closed orbit displacement calculation. A dipole kick $\Delta\theta_1$ at location 1 will lead to a closed orbit deviation (COD) Δx_2 at location 2:

$$\Delta\theta_1 = \frac{\Delta(BI)_1}{B\rho}$$

$$\Delta x_2 = \Delta\theta_1 \times \frac{\sqrt{\beta_1\beta_2}}{2\sin(\pi\nu)} \cos[\pi\nu - |\Psi_1 - \Psi_2|]$$

where $B\rho$ is the magnetic rigidity of the beam, ν is the tune, β and Ψ are the beta-function and phase advance, respectively. These expressions also provide a simple way to measure the beta function. If the steering magnet and BPM are close enough so that $\beta_1 \approx \beta_2 \approx \beta$, $\Psi_1 \approx \Psi_2$, then

$$\beta = 2 \times \tan(\pi\nu) \times B\rho \times \left(\frac{\Delta(BI)}{\Delta I} \right)^{-1} \times \left(\frac{\Delta x}{\Delta I} \right)$$

where $\Delta(BI)/\Delta I$ is the MI steering magnet strength, which takes the following values:

$$\Delta(BI)/\Delta I \text{ (horizontal)} = 0.007157 \text{ T-m/A}$$

$$\Delta(BI)/\Delta I \text{ (vertical)} = 0.003166 \text{ T-m/A}$$

Δx is the BPM response to a current change ΔI in the steering magnet. To create a local 3-bump, the sum of the three kicks must equal zero:

$$\theta_1 + \theta_2 + \theta_3 = 0$$

The required current ratios are:

$$I_2 = -I_1 \left(\frac{\beta_1}{\beta_2} \right)^{1/2} \frac{\sin(\Psi_1 - \Psi_3)}{\sin(\Psi_2 - \Psi_3)}$$

$$I_3 = I_1 \left(\frac{\beta_1}{\beta_3} \right)^{1/2} \frac{\sin(\Psi_1 - \Psi_2)}{\sin(\Psi_2 - \Psi_3)}$$

The reference orbit is shown in Figures 9 (horizontal) and 10 (vertical). A typical closed orbit deviation is shown in Figure 11. There are large orbit deviations at the WQBs, which are listed in Table 8. They are necessary because of the beam position shown in Figure 1.

Table 8: Reference Closed Orbit at WQBs

Q101	Q222	Q321	Q402	Q522	Q608	Q620
-19.52mm (V)	15.03mm (H)	-0.0994mm (V)	-26.38mm (H)	-25.31mm (H)	-31.93mm (H)	-33.69mm (H)

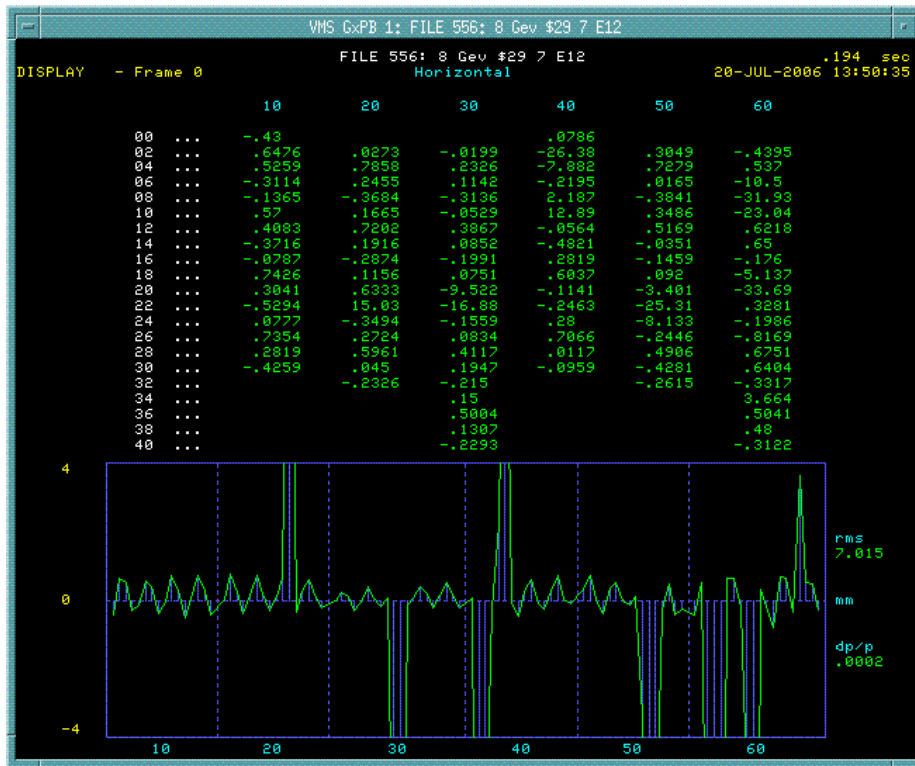


Figure 9: Reference closed orbit (horizontal).

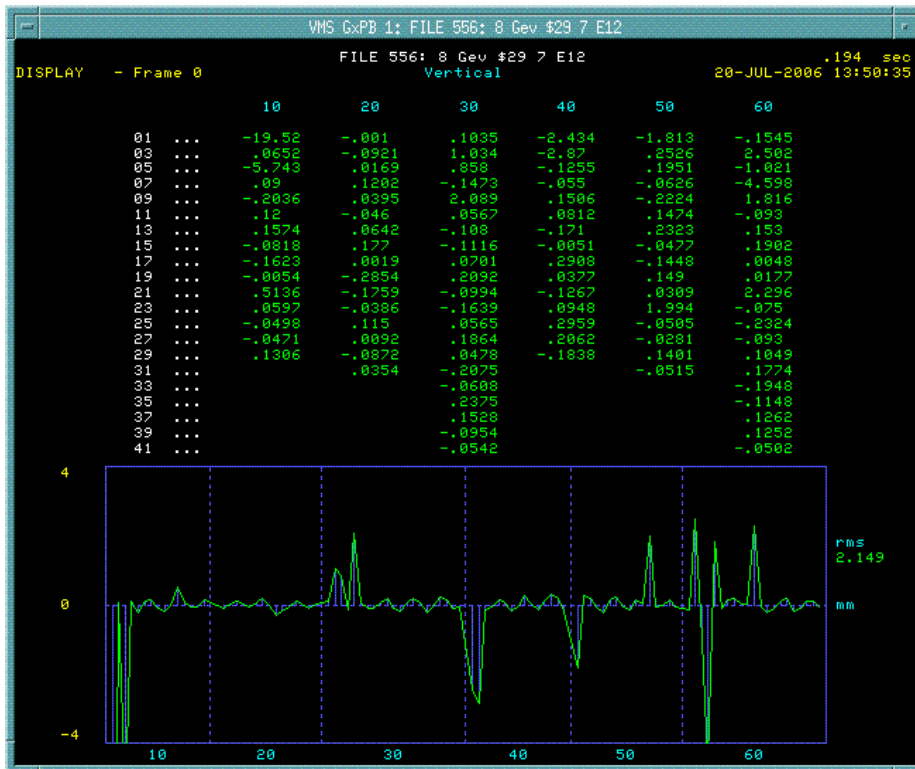


Figure 10: Reference closed orbit (vertical).

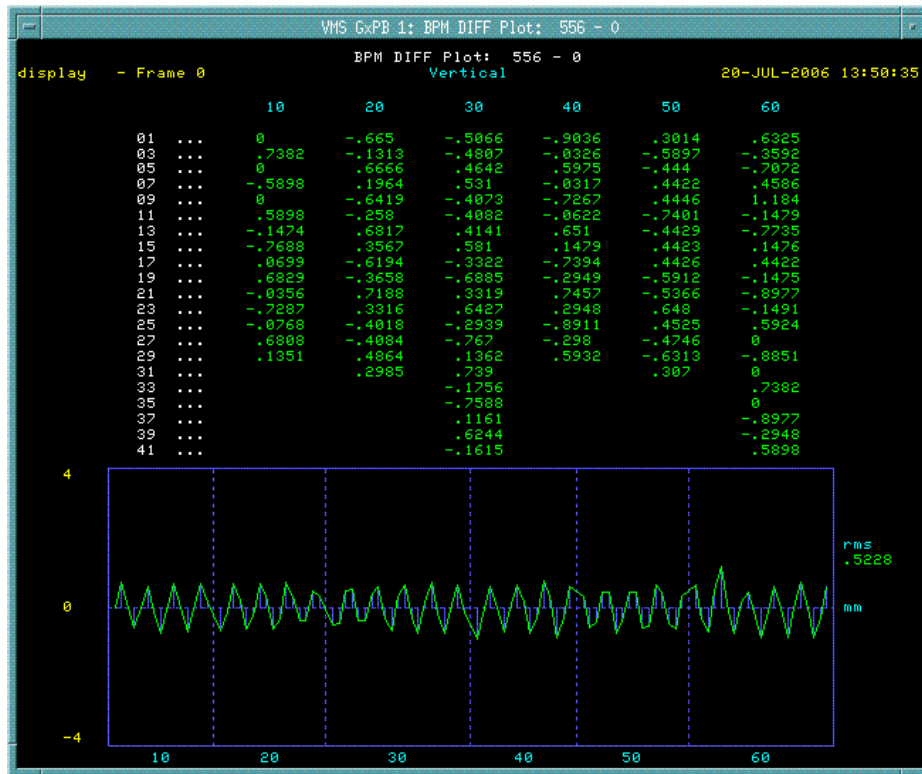


Figure 11: A typical closed orbit deviation (V101 – 0.25 A).

The 3-bump and 1-bump orbit measurements were compared to the MAD lattice model. The results are listed in Tables 9-11. The agreement between the predicted and measured closed orbit deviation in 3-bump is satisfactory. The biggest difference is about 0.5 mm at HP402, which could be attributed to the combination of lattice error, tune error, BPM data scaling polynomial error and non-linearity of the BPM at large amplitude.

The agreement for 1-bump, however, is not as good, especially at HP620, where the lattice model and measurement have significant difference. It is under investigation. The reason for better 3-bump results than 1-bump is probably the error cancellation when three CODs are summed up.

Table 9: Comparison of 3-Bump Measurement and MAD Lattice Model
(Courtesy P. Prieto)

Location	MAD β (m)	MAD Ψ ($\times 2\pi$)	Kick ratio (calc.)	COD (calc.) (mm/0.25A)	COD (meas.) (mm/0.25A)
V641	39.060	-0.132	1.0000		
V101	56.360	0.115	-0.1208		
VP101	56.668	0.122		1.25	1.48
V103	34.833	0.345	1.0672		
H220	53.630	6.349	1.0000		
H222	52.917	6.607	-0.0893		
HP222	53.400	6.613		3.21	3.44
H224	41.778	6.835	1.1425		
V319	49.462	9.89	1.0000		
V321	58.773	10.136	-0.2100		
VP321	59.233	10.142		1.43	1.56
V323	39.392	10.354	1.1432		
H400	51.912	13.208	1.0000		
H402	39.483	13.453	0.0723		
HP402	54.614	13.472		3.22	3.75
H404	54.357	13.718	0.9811		
H520	53.630	19.561	1.0000		
H522	38.311	19.807	-0.1041		
HP522	52.918	19.826		3.17	
H524	41.778	20.047	1.1349		
H606	53.300	21.852	1.0000		
H608	55.558	22.103	-0.0989		
HP608	55.888	22.109		3.28	
H610	39.509	22.336	1.1681		
H618	38.616	23.396	1.0000		
H620	38.206	23.646	-0.0696		
HP620	55.753	23.626		2.78	
H622	54.029	23.885	0.8474		

Table 10: Comparison of 1-Bump Measurement and MAD Lattice Model ($\Delta I > 0$)

Location	MAD β (m)	MAD Ψ ($\times 2\pi$)	COD (calc.) (mm/0.25A)	COD (meas.) (mm/0.25A)	COD (calc.) (mm/0.5A)	COD (meas.) (mm/0.5A)
V101	56.360	0.115				
VP101	56.668	0.122	-0.1735	-0.2965	-0.3470	-0.2965
VP321	59.233	10.142	-0.2717	-0.3512	-0.5435	-0.7025
V321	58.773	10.136				
VP101	56.668	0.122	-0.2105	0	-0.4211	-0.2965
VP321	59.233	10.142	-0.1762	-0.2321	-0.3524	-0.6183
H222	52.917	6.607				
HP222	53.400	6.613	0.4618	0.4632	0.9236	0.8246
HP402	54.614	13.472	-0.9481	-0.9872	-1.8962	-2.003
HP522	52.918	19.826	1.6439	1.646	3.2877	3.44
HP608	55.888	22.109	-0.4315	-0.6631	-0.8629	-0.6631
HP620	55.753	23.626	0.6026	1.272	1.2053	1.935
H402	39.483	13.453				
HP222	53.400	6.613	-0.9839	-1.003	-1.9678	-2.073
HP402	54.614	13.472	0.5152	0.6795	1.0304	1.346
HP522	52.918	19.826	0.7463	0.6002	1.4926	1.478
HP608	55.888	22.109	-1.3749	-2.545	-2.7498	-3.714
HP620	55.753	23.626	1.4181	2.617	2.8361	4.041
H522	38.311	19.807				
HP222	53.400	6.613	1.3989	1.442	2.7978	2.823
HP402	54.614	13.472	1.0120	1.18	2.0241	2.23
HP522	52.918	19.826	0.4996	0.4751	0.9991	1.11
HP608	55.888	22.109	1.2101	1.384	2.4202	2.848
HP620	55.753	23.626	-1.1188	-1.203	-2.2376	-2.341
H608	55.558	22.103				
HP222	53.400	6.613	-0.3075	-0.1182	-0.6150	-0.1999
HP402	54.614	13.472	-1.5017	-1.217	-3.0034	-2.463
HP522	52.918	19.826	1.5434	1.408	3.0868	3.014
HP608	55.888	22.109	0.4841	0.6821	0.9682	1.384
HP620	55.753	23.626	-0.6579	-0.6097	-1.3159	-1.203
H620	38.206	23.646				
HP222	53.400	6.613	0.6145	0.6193	1.2290	1.169
HP402	54.614	13.472	1.3827	1.593	2.7654	3.143
HP522	52.918	19.826	-1.0829	-1.335	-2.1659	-2.512
HP608	55.888	22.109	-0.6610	-0.6631	-1.3219	-1.935
HP620	55.753	23.626	0.5205	1.272	1.0410	1.935

Table 11: Comparison of 1-Bump Measurement and MAD Lattice Model ($\Delta I < 0$)

Location	MAD β (m)	MAD Ψ ($\times 2\pi$)	COD (calc.) (mm/-0.25A)	COD (meas.) (mm/-0.25A)	COD (calc.) (mm/-0.5A)	COD (meas.) (mm/-0.5A)
V101	56.360	0.115				
VP101	56.668	0.122	0.1831	0	0.3661	0.312
VP321	59.233	10.142	0.2814	0.3319	0.5628	0.7236
V321	58.773	10.136				
VP101	56.668	0.122	0.2203	0	0.4406	0.312
VP321	59.233	10.142	0.1862	0.3292	0.3724	0.5279
H222	52.917	6.607				
HP222	53.400	6.613	-0.4688	-0.4744	-0.9375	-0.7809
HP402	54.614	13.472	0.9435	1.062	1.8869	2.135
HP522	52.918	19.826	-1.6452	-1.764	-3.2904	-3.55
HP608	55.888	22.109	0.4386	0.6631	0.8772	0.6631
HP620	55.753	23.626	-0.6097	0	-1.2194	-0.6097
H402	39.483	13.453				
HP222	53.400	6.613	0.9807	1.477	1.9613	2.112
HP402	54.614	13.472	-0.5213	-0.8037	-1.0425	-1.082
HP522	52.918	19.826	-0.7421	-0.4471	-1.4842	-1.589
HP608	55.888	22.109	1.3783	1.345	2.7567	4.276
HP620	55.753	23.626	-1.4209	-1.78	-2.8419	-2.887
H522	38.311	19.807				
HP222	53.400	6.613	-1.4009	-1.32	-2.8019	-2.835
HP402	54.614	13.472	-1.0090	-1.139	-2.0180	-2.219
HP522	52.918	19.826	-0.5054	-0.6965	-1.0109	-1.26
HP608	55.888	22.109	-1.2082	-1.881	-2.4163	-3.612
HP620	55.753	23.626	1.1162	1.935	2.2325	3.319
H608	55.558	22.103				
HP222	53.400	6.613	0.3146	0.2581	0.6293	0.2631
HP402	54.614	13.472	1.5066	1.359	3.0132	2.637
HP522	52.918	19.826	-1.5422	-1.501	-3.0844	-3.026
HP608	55.888	22.109	-0.4914	-1.272	-0.9828	-1.881
HP620	55.753	23.626	0.6652	1.935	1.3303	2.617
H620	38.206	23.646				
HP222	53.400	6.613	-0.6203	-0.5655	-1.2406	-1.143
HP402	54.614	13.472	-1.3855	-1.533	-2.7709	-3.018
HP522	52.918	19.826	1.0804	1.132	2.1608	2.51
HP608	55.888	22.109	0.6668	0.6631	1.3337	2.047
HP620	55.753	23.626	-0.5265	0	-1.0530	-0.6097

7. Machine Aperture and Acceptance Improvement

The reason to replace the regular quads by WQBs is to increase the aperture in the bottleneck locations. Figure 12 shows the cross section of the Lambertson magnet, the old beam pipe for the IQB and new pipe for the WQB. It is seen that the expected aperture increase is about 10 mm. This was verified by aperture scanning. Figure 13 shows the scanning results at Q608. It was done using a low intensity beam for one turn circulation. Beam was immediately dumped after one turn. Therefore, it measured the clean physical aperture that had zero beam loss and excluded the effect of the magnet good field region, which would give rise to the dynamic aperture.

Figure 14 shows the WQB increases the machine acceptance to 60π mm-mrad. Compared with 40π mm-mrad before, the increase is 50%. Further increase is possible because the acceptance is indeed limited by the good field region (51 mm or 2") rather than physical aperture. If the Lambertson magnet is moved by 10 mm, one can make full use of the large aperture and increase the acceptance to 80π mm-mrad, as demonstrated in Figure 15.

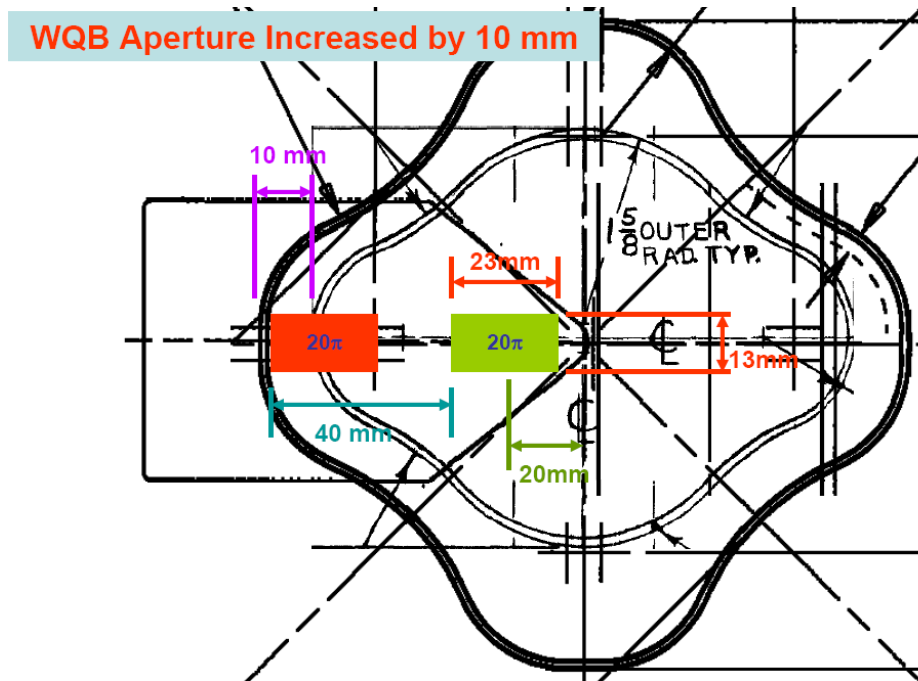


Figure 12: The Lambertson magnet aperture, the old beam pipe and the new beam pipe. The horizontal aperture is increased by 10 mm.



Figure 13: Aperture scanning near Q608. The zero-loss aperture is about 10 mm larger than that of the regular quad measured before. (Courtesy M. Yang)

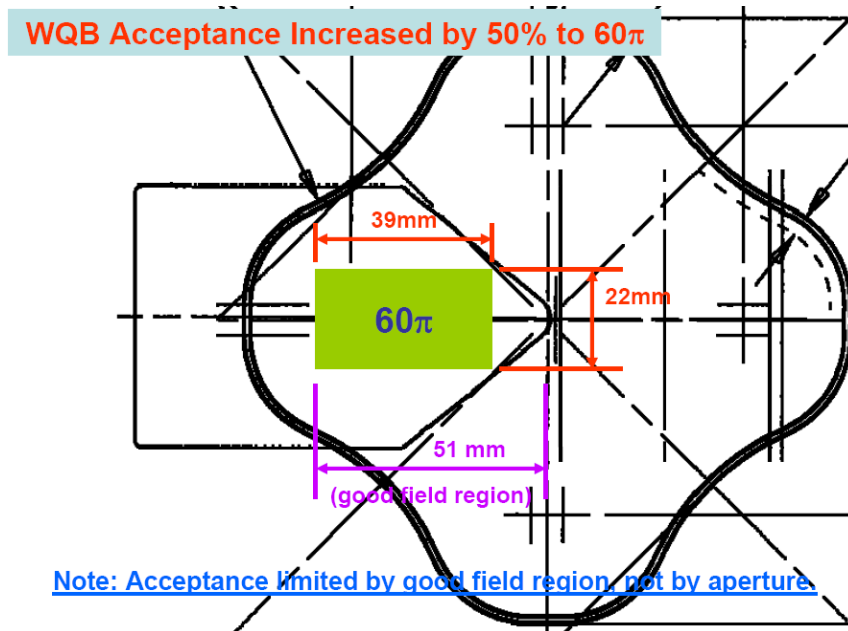


Figure 14: The machine acceptance is increased from 40π (see Fig. 1) to 60π . The acceptance is limited by the good field region of the WQB.

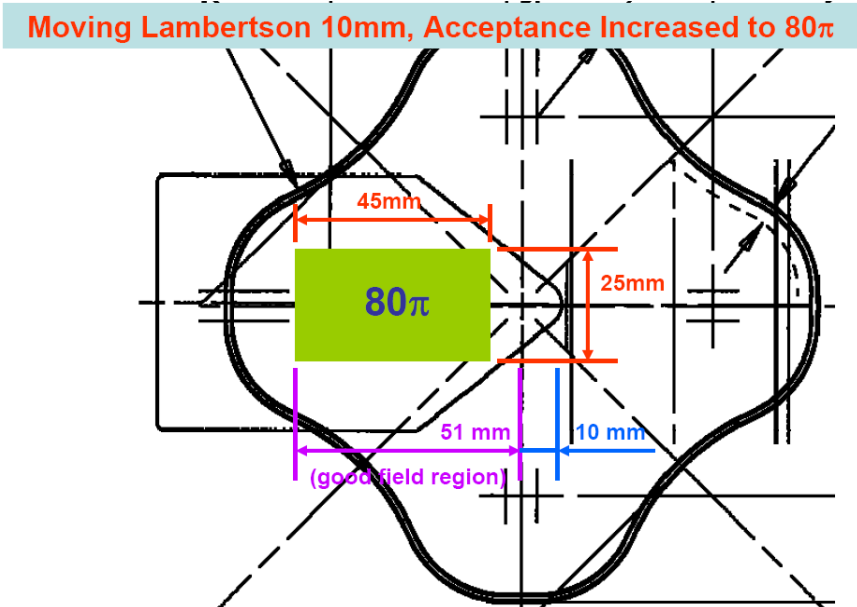


Figure 15: Illustration of further acceptance increase to 80π by moving the Lambertson magnet by 10 mm.

8. Acknowledgement

The WQB project involved a good number of people from the Technical Division and Accelerator Division. Their hard work in the past two years made the project a success. The work at the Technical Division was under the leadership of D. Harding, and I. Kourbanis provided guidance to the work at the Accelerator Division. W. Chou served as a liaison. The participants included (in alphabetical order): M. Albertus and his installation group, L. Alsip, R. Andrews, L. Bartelson, J. Blowers, B. Brown, D. Capista, J. Crisp, J. DiMarco, J. Fitzgerald, T. J. Gardner, H. Glass, B. Hendricks, D. Johnson, V. Kashikhin, L. Nobrega, F. Ostiguy, P. Prieto, B. Robotham, T. Sager and C. Wilson and their survey group, M. Tartaglia, L. Valerio, R. Webber, D. White, D. Wolff, M. Yang and J. Zweibohmer. The project was funded by the Proton Plan in the Accelerator Division.

9. References

- [1] <http://tdserver1.fnal.gov/AcceleratorSupport/Magnets/Quadrupoles/WQB/>
- [2] R. Webber, "MI BPM Cable Measurement," Beams Document 2288, Accelerator Division Database, Fermilab (2006).
- [3] W. Chou, "Derivation of the S-Curve of BPM Signals," APS/IN/ACCPHY/89-3, APS Project, Argonne National Laboratory (1989).
- [4] R. Webber, "MI Extra Wide Aperture BPM Scaling in Difference-Over-Sum BPM System," Beams Document 2280, Accelerator Division Database, Fermilab (2006).

Appendix: Locations and End Views of the Installed WOBs

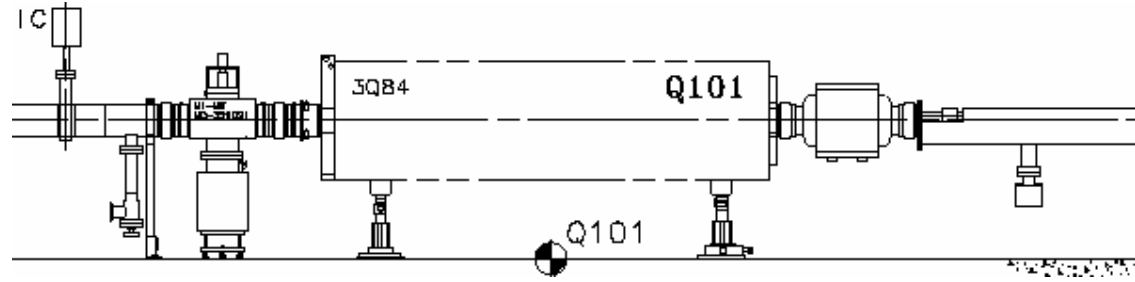


Figure 16: Q101 – WQB 001, EXWA BPM 01

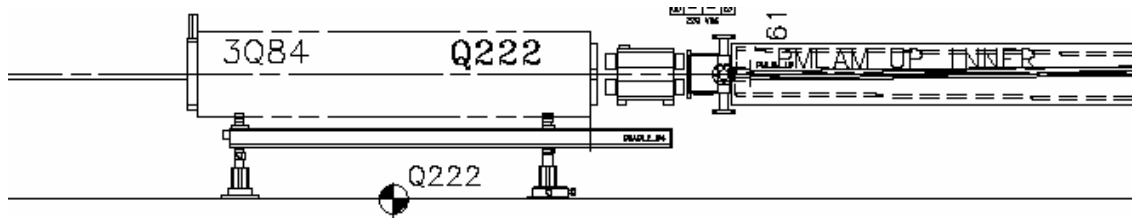


Figure 17: Q222 – WQB 007, EXWA BPM 07

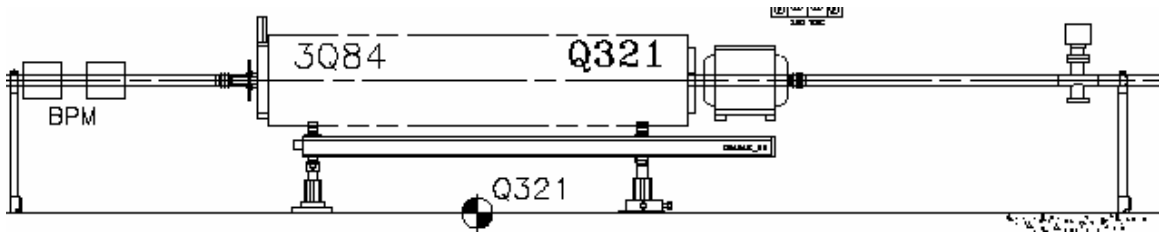


Figure 18: Q321 – WQB 006, EXWA BPM 08

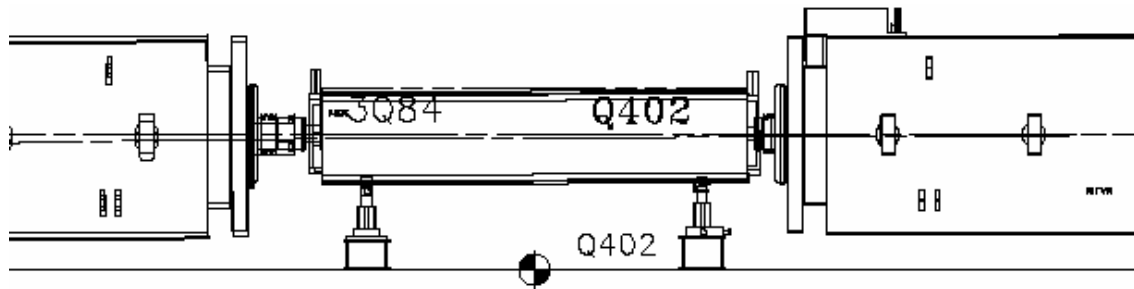


Figure 19: Q402 – WQB 004, EXWA BPM 04

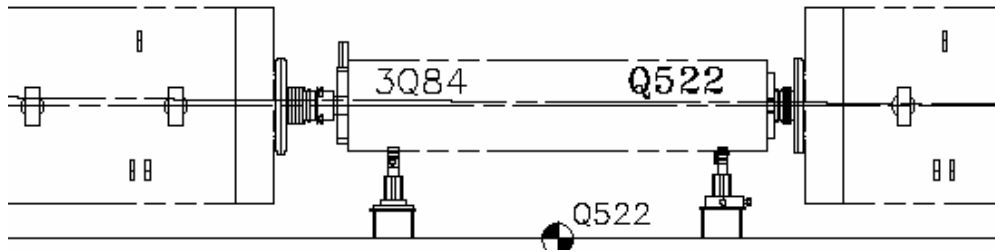


Figure 20: Q522 – WQB 003, EXWA BPM 02

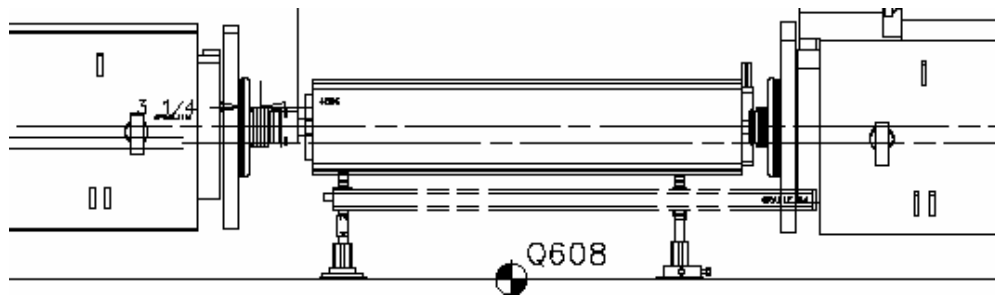


Figure 21: Q608 – WQB 005, EXWA BPM 05

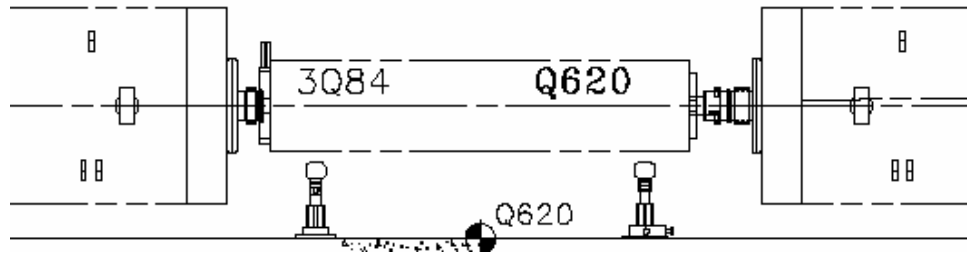


Figure 22: Q620 – WQB 002, EXWA BPM 06